

Towards ultra-stiff materials: Surface effects on nanoporous materials

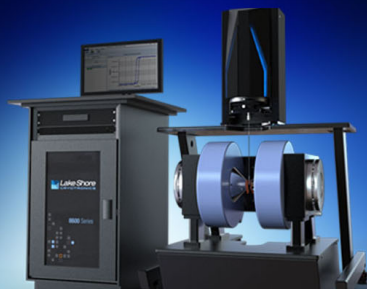
Dingjie Lu, Yi Min Xie, Qing Li, Xiaodong Huang, and Shiwei Zhou*

Citation: *Appl. Phys. Lett.* **105**, 101903 (2014); doi: 10.1063/1.4895582

View online: <http://dx.doi.org/10.1063/1.4895582>


View Table of Contents: <http://aip.scitation.org/toc/apl/105/10>

Published by the [American Institute of Physics](#)



NEW 8600 Series VSM

For fast, highly sensitive
measurement performance

LEARN MORE 

Towards ultra-stiff materials: Surface effects on nanoporous materials

Dingjie Lu,¹ Yi Min Xie,¹ Qing Li,² Xiaodong Huang,¹ and Shiwei Zhou^{1,a)}

¹Centre for Innovative Structures and Materials, School of Civil, Environmental and Chemical Engineering, RMIT University, GPO Box 2476, Melbourne 3001, Australia

²School of Aerospace, Mechanical and Mechatronics Engineering, The University of Sydney, New South Wales 2006, Australia

(Received 13 July 2014; accepted 30 August 2014; published online 11 September 2014)

The significant rise in the strength and stiffness of porous materials at nanoscale cannot be described by conventional scaling laws. This letter investigates the effective Young's modulus of such materials by taking into account surface effect in a microcellular architecture designed for an ultralight material whose stiffness is an order of magnitude higher than most porous materials. We find that by considering the surface effects the predicted stiffness using Euler-Bernoulli beam theory compares well to experimental data for spongelike nanoporous gold with random microstructures. Analytical results show that, of the two factors influencing the effective Young's modulus, the residual stress is more important than the surface stiffness. © 2014 AIP Publishing LLC.

[<http://dx.doi.org/10.1063/1.4895582>]

Many remarkable features of nanoporous materials are largely attributed to the high surface area to volume ratio of their microstructure at nanometer scale. Due to strong interactions of molecules and their clusters on such a large surface,¹⁻³ the dependence of Young's modulus and yield stress on the relative density for nanoporous materials cannot be described by conventional scaling laws,⁴ which are typically applicable to porous materials whose cell sizes are larger than 100 μm . Unfortunately, the structure-property relationships for nanoporous materials remain open questions.⁵⁻⁸

Recent advances in the continuum theory of surface elasticity⁹ have opened a new window to studying the size-dependent phenomena at nanoscale.¹⁰⁻¹⁴ A framework of surface elasticity theory was established to evaluate the elastic behaviour of static bending nanowires, indicating that they become softer or stiffer under different boundary conditions.¹² The combination of Gurtin's method⁹ with Euler-Bernoulli and Timoshenko beam theories provides an adequate technique to determine the surface effects on the elastic properties of nanoporous materials.^{5,15} Up to date, the fundamental models that have been considered are mainly restricted to an orthogonal structure consisting of only horizontal and vertical beams as shown in Fig. 1(a). This structure was conceived for the convenience of deformation analysis rather than efficient material utilization which is of considerable significance to the effective properties of low-density porous materials.^{16,17} Therefore, we would like to investigate a microcellular architecture (Fig. 1(b)), which was designed to increase the effective Young's modulus E^* .¹⁸ Such an elegant architecture constitutes an ultra light-weight porous material with $E^* \sim (\rho/\rho_0)^2$ (ρ and ρ_0 denote density of porous and bulk/base materials), distinguished from traditional $E^* \sim (\rho/\rho_0)^3$ for its stochastic counterparts.

The investigation into the effective Young's modulus based on the model proposed in Fig. 1(b) will benefit the understanding of exceptional performance of nanoporous materials, which are more commonly composed of inclined

beams. In this letter, we combine the classical solution to Euler-Bernoulli beam theory with the surface elasticity theory to quantify E^* at nanoscale. The Young-Laplace equation¹⁹ and the surface elasticity model⁹ are used to evaluate the effects of surface tension and surface elasticity. In addition, the Euler-Bernoulli beam theory,²⁰ which neglects the longitudinal extension of the nanostrut, is utilized to analyze the deflection of struts imposed by distributed transverse load due to the surface effects. The representative element (unit cell) of the porous material is a diamond-like cell consisting of eight identical struts as shown in Fig. 1(b), where L and $\theta = \pi/3$ denote the strut length and the angle with respect to the horizontal direction, respectively. The strut has a solid circular cross section with diameter D and the unit cell is subjected to stress σ vertically.

The interactions of superficial resident constraints with the interior atoms lead to surface tension and a stress jump across the interface, which is termed as surface effects generally existing in nanostructures.²¹ Such effects can be simplified by surface stress caused by transverse load on the edge of nanostruts along normal direction in terms of the generalized Young-Laplace equation and Gurtin's theory of surface elasticity,²¹⁻²³ given as

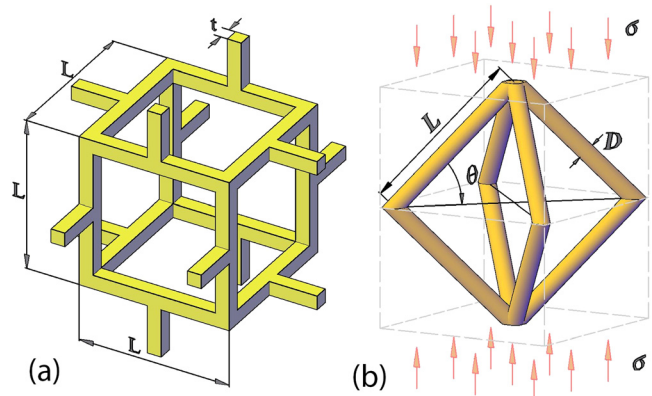


FIG. 1. (a) The classical orthogonal cell model. (b) A schematic of the octahedral cell composed of inclined struts.

^{a)}Electronic mail: shiwei.zhou@rmit.edu.au

$$\sigma_{\alpha\beta}^s = \gamma\delta_{\alpha\beta} + \partial\gamma/\partial\varepsilon_{\alpha\beta}^s, \quad (1)$$

where $\delta_{\alpha\beta}$ is the Kronecker delta and γ is the surface energy. The surface strain tensor $\varepsilon_{\alpha\beta}^s$ is assumed to be the tangential strain tensor. According to Eq. (1) and under the assumption that the surface of the nanostrut is homogeneous, isotropic, and linearly elastic,²⁴ the overall surface stress τ along the longitudinal direction of strut is

$$\tau = \tau_0 + E_s\varepsilon_s, \quad (2)$$

where τ_0 is the residual surface stress at the strain-free state and ε_s is the longitudinal surface strain. The stiffness of the surface layer is denoted as E_s . According to Young-Laplace equation, the stress jump $\Delta\sigma_{ij}$ across the interface depends on the surface curvature $\kappa_{\alpha\beta}$ and surface stress $\tau_{\alpha\beta}$,^{19,24,25} given as

$$\Delta\sigma_{ij}n_in_j = \tau_{\alpha\beta}\kappa_{\alpha\beta}, \quad (3)$$

where n_i and n_j denote the unit normal vectors.

Based on Eqs. (2) and (3), the surface effects with consideration of residual surface stress are converted into distributed load along the transverse direction of the beam as shown in Fig. 2, given as

$$p(x) = H\kappa. \quad (4)$$

From Euler-Bernoulli beam theory, the mean curvature $\kappa = v''$ is the second derivative of the small deflection v and variable H is integrated along the edge of cross section as

$$H = 2 \int_{-\pi/2}^{\pi/2} (D/2)\tau \cos\theta d\theta = 2\tau D. \quad (5)$$

The equilibrium equation for the bending strut under the distributed force $p(x)$ is

$$(EI)^*v'''' = p(x). \quad (6)$$

When $t \ll D$, the flexural stiffness, according to the composite beam theory,²⁰ is

$$\begin{aligned} (EI)^* &= EI + E_1 \int_0^{2\pi} ((D/2)\cos\theta)^2 (D/2)t d\theta \\ &= EI + \frac{\pi}{8}E_s D^3, \end{aligned} \quad (7)$$

where $I = \pi D^4/64$ is the second moment of inertia of circular cross section. In our model, the elastic modulus $E_1 = E_s/t$ of

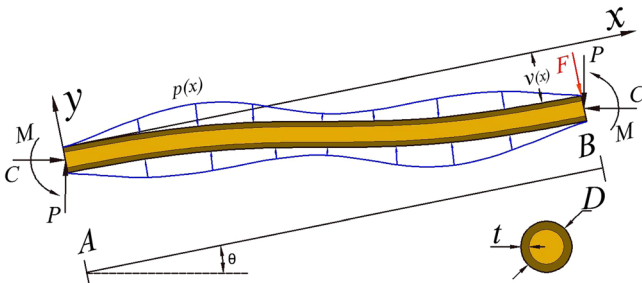


FIG. 2. The free-body diagram and its deflection for a typical inclined strut under compression stress σ and the distributed load $p(x)$ caused by surface effects.

the surface layer with a thickness of t is governed by the surface elasticity model while the inner bulk volume obeys the conventional continuum mechanics theory.^{26–28} Under small deformation the surface strain can be approximated as $\varepsilon_s \approx -(D/2)v''$. Substituting Eqs. (2) and (5) into Eq. (6) leads to

$$(EI)^*v'''' = p(x) = H\kappa \approx 2D(\tau_0 - E_s(D/2)v'')v''. \quad (8)$$

After neglecting the higher order term $(v'')^2$, Eq. (8) is simplified as

$$(EI)^*v'''' \approx 2D\tau_0v'' = H^0v''. \quad (9)$$

Figure 2 schematically shows the free-body diagram for a typical inclined strut and its deflection v . As discussed above, distributed load $p(x)$ is imposed on the normal direction and its magnitude depends on the mean curvature. Force F and moment M induced by stress σ are applied at both ends. The cross section of the beam having thickness t of the layer with surface effects is illustrated in the inset of Fig. 2. Based on equilibrium equations, these forces can be simply obtained as

$$C = 0, \quad (10)$$

$$P = (\sqrt{2}L \cos\theta + D)^2\sigma/4, \quad (11)$$

$$M = L \cos\theta(\sqrt{2}L \cos\theta + D)^2\sigma/8, \quad (12)$$

$$F = \cos\theta(\sqrt{2}L \cos\theta + D)^2\sigma/4. \quad (13)$$

The deflection and slope at the fixed left end are

$$v(0) = v'(0) = 0. \quad (14)$$

Due to the symmetry of the geometry and loads, the curvature at the middle of the beam with $x = L/2$ is

$$v''(L/2) = 0. \quad (15)$$

By integrating the transverse load $p(x)$ in Eq. (9) from $x = \alpha$ to $x = L$ ($\alpha \in (0, L)$), we obtain the force equilibrium as

$$-(EI)^*v'''(\alpha) = P + \int_{\alpha}^L H^0v'' dx = F + H^0(v'(L) - v'(\alpha)). \quad (16)$$

With the consideration of boundary conditions (Eqs. (14)–(16)) in Eq. (6), the deflection is determined as

$$\begin{aligned} v(x) &= \frac{F(3L - 2x)x^2}{12(EI)^*}, \quad \tau_0 = 0, \quad (17) \\ v(x) &= \frac{F(e^{(L-x)\eta} - e^{x\eta} + e^{L\eta}(x\eta - 1) + x\eta + 1)}{H^0(e^{L\eta} + 1)\eta}, \quad \tau_0 \neq 0, \end{aligned} \quad (18)$$

where $\eta = \sqrt{H^0/(EI)^*}$ is a symbol to simplify the formula. It is noted that Eq. (17) becomes the classical Euler-Bernoulli beam theory when $E_s = 0$ and Eq. (18) is equal to Eq. (17) when $\tau_0 = 0$.

The component $v \cos \theta$ of deflection in the direction of σ divided by the vertical projection $L \sin \theta$ of length L gives

$$\varepsilon = v(L) \cos \theta / (L \sin \theta). \quad (19)$$

Thus, the effective Young's modulus $E^* = \sigma/\varepsilon$ is obtained as

$$E^* = \frac{48(EI)^* \sin \theta}{((\sqrt{2}L \cos \theta + D)L \cos \theta)^2}, \quad \tau_0 = 0, \quad (20)$$

$$E^* = \frac{4H^0L \sin \theta}{((\sqrt{2}L \cos \theta + D) \cos \theta)^2 \left(\frac{2}{\eta} \tanh\left(-\frac{L\eta}{2}\right) + L \right)}, \quad \tau_0 \neq 0 \quad (21)$$

The ratio of D to L can be related to the relative density as $D/L = c\sqrt{\rho/\rho_0}$, where $c \approx 1$ is a topology-dependent factor for most porous materials with open cells.³² For the cell shown in Fig. 1(b), we calculate $c = \sqrt{2 \cos^2 \theta \sin \theta / \pi}$. Without loss of generality, the relative density is assumed to be $\rho/\rho_0 = 31\%$ in the following discussions,² a representative value for porous material. Nanoporous gold (np-Au) is used to embody the effective Young's modulus in Eqs. (20) and (21) as it has been fabricated by dealloying method² with the ligament size ranging from a few nanometers to $1 \mu\text{m}$. Moreover the size-dependent behaviours of np-Au with relative densities from 20% to 42% has been tested,²⁹ which can be used as a reliable criterion to evaluate the analysis results. This letter mainly focuses on the stiffness so other superior physical properties and unique functions of np-Au are not considered. For the single-crystalline gold, $E_0 = 70 \text{ GPa}$, $\tau_0 = 1.40 \text{ N/m}$, and $E_s = 3.63 \text{ N/m}$ on the (001) crystal surface are calculated from ideal atomic simulation.³³ However, small ligament size leads to a dramatic increase in residual stress,³¹ In addition, some post-fabrication processes such as annealing also result in higher residual stress. Therefore, it is plausible to let $\tau_0 = 80 \text{ N/m}$ in Eq. (21).

Figure 3 depicts the dependence of E^* on D . It clearly shows that the effective values (the red curve with square markers) well match the experimental data (five black stars in Fig. 3) for np-Au with similar (001) crystal surface properties.²⁹ The blue curve with triangle markers in Fig. 3 is for the classical Gibson and Ashby's cell with similar parameters except for $c = 1$. It shows the effective values⁵ are much

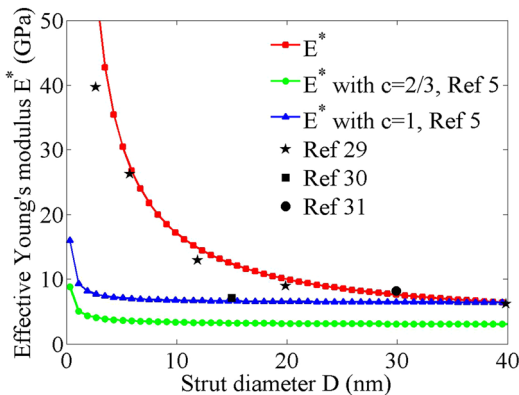


FIG. 3. The comparison of E^* in terms of octahedral unit cell as well as Gibson and Ashby's model⁵ with experimental data ($E_s = 3.63 \text{ N/m}$, $\tau_0 = 80 \text{ N/m}$, $\rho/\rho_0 = 31\%$).²⁹⁻³¹

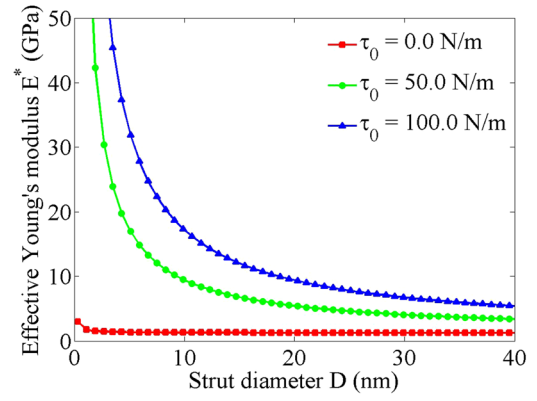


FIG. 4. Effect of residual surface stress on E^* with $E_s = 3.63 \text{ N/m}$ and $\rho/\rho_0 = 31\%$.

lower than the experimental data for small ligament size. According to our model and experimental data, the surface effect becomes discernible when the ligament size is smaller than 20 nm while Gibson and Ashby's model does not show this effect until the ligament size is less than 3 nm . The green curve with circle markers in Fig. 3 is for $c = 2/3$, an exact calculation for Gibson and Ashby's cell, but it deviates from the experimental results further. The black square³⁰ and black circle markers³¹ stand for the experimental data for np-Au from other references, which are within an acceptable error margin in comparison with our analytical results.

Because the residual stress is significantly influenced by the fabrication techniques and the surface stiffness varies with different crystal surfaces, the effects of τ_0 and E_s on E^* are presented in Figs. 4 and 5, respectively. Both figures illustrate that the increase of each factor leads to higher E^* , in particular, when the strut size is less than 10 nm . However, it seems that τ_0 plays a more significant role in affecting E^* than E_s when the ligament size $D > 3 \text{ nm}$. It is noted in Fig. 4 that the critical point of surface effects changes from 1 nm to 10 nm for the ligament size when τ_0 increases from 0 to 50 N/m . The role of τ_0 on intensifying the surface effects becomes weaker for larger residual stress as shown in the blue curve with triangle markers for $\tau_0 = 100$, which is only marginally higher than the green curve with circular markers for $\tau_0 = 50 \text{ N/m}$ in Fig. 4. Compared with the residual stress, the surface stiffness is

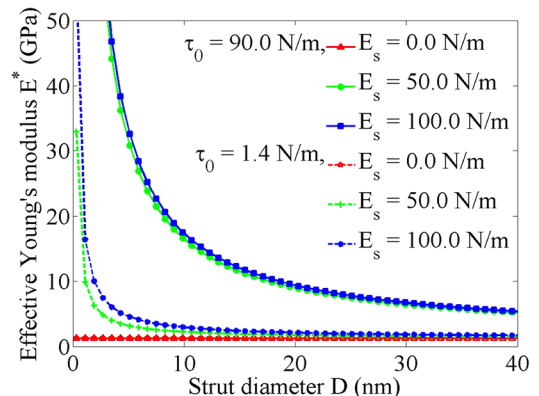


FIG. 5. Effect of surface stiffness on E^* with $\tau_0 = 1.4 \text{ N/m}$ and $\tau_0 = 90 \text{ N/m}$ for $\rho/\rho_0 = 31\%$.

less important because the doubling of E_s from 50 N/m to 100 N/m slightly changes E^* in Fig. 5. If $\tau_0 = 1.4$ N/m, the role of E_s is negligible unless $D < 1$ nm. Thus, it is more reasonable to attribute the rise of E_s in Fig. 5 to higher value of $\tau_0 = 90$ N/m than to $E_s = 50$ N/m or $E_s = 100$ N/m.

In conclusion, this work has studied the surface effects on the effective Young's modulus for a model with inclined struts, which is more akin to the microstructure of nanoporous materials. Gurtin's theory and Young-Laplace equation are used in combination with Euler-Bernoulli beam theory to obtain an explicit definition to the effective Young's modulus of nanoporous gold. Analytical solution clearly demonstrates the experimentally observed surge of Young's modulus at nanoscale for nanoporous gold.²⁹ It also reveals that the residual surface tension plays a more important role than the stiffness of surface layer. Our study affirms that the architecture of microstructure could significantly impact on the overall behaviour of nanoporous materials, and it is possible to optimize the base cell by using structural topology optimization techniques in order to improving the effective Young's modulus.

The work was funded by Australian Research Council (DE120102906 and DP110104698).

- ¹J. Weissmüller, R. C. Newman, H. J. Jin, A. M. Hodge, and J. W. Kysar, *MRS Bull.* **34**, 577 (2009).
- ²A. M. Hodge, J. Biener, J. R. Hayes, P. M. Bythrow, C. A. Volkert, and A. V. Hamza, *Acta Mater.* **55**, 1343 (2007).
- ³R. Dou, B. Xu, and B. Derby, *Scr. Mater.* **63**, 308 (2010).
- ⁴L. Gibson and M. Ashby, *Cellular Solids: Structure and Properties* (Cambridge University Press, 1999).
- ⁵X. Q. Feng, R. Xia, X. Li, and B. Li, *Appl. Phys. Lett.* **94**, 011916 (2009).
- ⁶J. Biener, A. M. Hodge, A. V. Hamza, L. M. Hsiung, and J. H. Satcher, *J. Appl. Phys.* **97**, 024301 (2005).
- ⁷P. Armstrong and W. Peukert, *J. Nanopart. Res.* **14**, 1288 (2012).
- ⁸H. F. Zhan and Y. T. Gu, *J. Appl. Phys.* **111**, 084305 (2012).

- ⁹M. E. Gurtin, J. Weissmüller, and F. Larch, *Philos. Mag. A* **78**, 1093 (1998).
- ¹⁰T. Y. Zhang, M. Luo, and W. K. Chan, *J. Appl. Phys.* **103**, 104308 (2008).
- ¹¹J. S. Wang, X. Q. Feng, G. F. Wang, and S. W. Yu, *Appl. Phys. Lett.* **92**, 191901 (2008).
- ¹²J. He and C. M. Lilley, *Nano Lett.* **8**, 1798 (2008).
- ¹³X. F. Li, H. Zhang, and K. Y. Lee, *Int. J. Mech. Sci.* **81**, 120 (2014).
- ¹⁴X. P. Zheng, Y. P. Cao, B. Li, X. Q. Feng, and G. F. Wang, *Nanotechnology* **21**, 205702 (2010).
- ¹⁵R. Xia, X. Li, Q. Qin, J. Liu, and X. Q. Feng, *Nanotechnology* **22**, 265714 (2011).
- ¹⁶M. P. Bendos and O. Sigmund, *Topology Optimization - Theory, Methods, and Applications* (Springer Verlag, 2003).
- ¹⁷S. Sturm, S. W. Zhou, Y. Mai, and Q. Li, *J. Biomech.* **43**, 1738 (2010).
- ¹⁸T. A. Schaedler, A. J. Jacobsen, A. Torrents, A. E. Sorensen, J. Lian, J. R. Greer, L. Valdevit, and W. B. Carter, *Science* **334**, 962 (2011).
- ¹⁹T. Y. Chen, M. S. Chiu, and C. N. Weng, *J. Appl. Phys.* **100**, 074308 (2006).
- ²⁰J. Gere and S. Timoshenko, *Mechanics of Materials* (PWS-Kent Pub. Co., 1990).
- ²¹R. C. Cammarata and K. Sieradzki, *Annu. Rev. Mater. Sci.* **24**, 215 (1994).
- ²²T. Goudarzi, R. Avazmohammadi, and R. Naghdabadi, *Mech. Mater.* **42**, 852 (2010).
- ²³A. K. Miri, R. Avazmohammadi, and F. Yang, *J. Comput. Theor. Nanosci.* **8**, 231 (2011).
- ²⁴R. E. Miller and V. B. Shenoy, *Nanotechnology* **11**, 139 (2000).
- ²⁵G. F. Wang and X. Q. Feng, *Appl. Phys. Lett.* **90**, 231904 (2007).
- ²⁶C. Q. Chen, Y. Shi, Y. S. Zhang, J. Zhu, and Y. J. Yan, *Phys. Rev. Lett.* **96**, 075505 (2006).
- ²⁷S. Cuenot, C. Fretigny, S. Demoustier-Champagne, and B. Nysten, *Phys. Rev. B* **69**, 165410 (2004).
- ²⁸G. Y. Jing, H. L. Duan, X. M. Sun, Z. S. Zhang, J. Xu, Y. D. Li, J. X. Wang, and D. P. Yu, *Phys. Rev. B* **73**, 235409 (2006).
- ²⁹A. Mathur and J. Erlebacher, *Appl. Phys. Lett.* **90**, 061910 (2007).
- ³⁰C. A. Volkert, E. T. Lilleodden, D. Kramer, and J. Weissmüller, *Appl. Phys. Lett.* **89**, 061920 (2006).
- ³¹D. Y. Lee, X. D. Wei, M. H. Zhao, X. Chen, S. C. Jun, J. Hone, and J. W. Kysar, *Modell. Simul. Mater. Sci. Eng.* **15**, S181 (2007).
- ³²J. Biener, A. M. Hodge, J. R. Hayes, C. A. Volkert, L. A. Zepeda-Ruiz, A. V. Hamza, and F. F. Abraham, *Nano Lett.* **6**, 2379 (2006).
- ³³V. B. Shenoy, *Phys. Rev. B* **71**, 094104 (2005).